Thermoelectric evidence of the electronic structure changes from the charge density wave transition in FeGe

Kaila Jenkins,[1] Yuan Zhu,[1] Dechen Zhang,[1] Guoxin Zheng,[1] Kuan-Wen Chen,[1] Aaron Chan,[1] Sijie Xu,[2,3] Mason L. Klemm,[2,3] Bin Gao,[2,3] Ming Yi,[2,3] Pengcheng Dai,[2,3] and Lu Li[1,*]

[1]*Department of Physics, University of Michigan, Ann Arbor, Michigan 48109, USA*

[2]*Department of Physics and Astronomy, Rice University, Houston, Texas 77005, USA*

[3]*Rice Laboratory for Emergent Magnetic Materials and Smalley-Curl Institute, Rice University, Houston, Texas 77005, USA*

(Received 26 August 2025; revised 10 February 2026; accepted 16 March 2026; published 8 April 2026)

Kagome metals provide a material platform for probing new correlated quantum phenomena due to the naturally incorporated linear dispersions, flat bands, and Van Hove singularities in their electronic structures. Among these quantum phenomena is the charge density wave (CDW), or the distortion of the lattice structure due to the motion of correlated electrons through the material. CDWs lower the energy of the compound, creating an energy gap that facilitates behaviors akin to superconductivity, nonlinear transport, or other quantum correlated phenomena. The kagome metal FeGe has been shown to host a CDW transition at approximately 100 K, and its occurrence is strongly influenced by the sample annealing conditions. However, a notable gap in the literature is the lack of clear thermoelectric transport evidence for electronic structure changes associated with this CDW transition. Here, we present evidence of electron behavior modification due to annealing disorder via thermoelectric measurements on FeGe crystals presenting a CDW transition and those without a CDW. The observed Nernst effect and Seebeck effects demonstrate pronounced modifications of electrical transport properties associated with CDW formation and its suppression by annealing-induced disorder, including a change in the thermopower sign and a strong enhancement of the Nernst response in the CDW state. Our results provide evidence of multiple phase transitions, which confirms the influence of CDW on the thermal properties of FeGe and demonstrates the suppression of CDW with sufficient disordering.

DOI: 10.1103/7rx9-12rw

I. INTRODUCTION

Novel electronic and magnetic materials have garnered considerable interest in recent years because of their environmental, technological, and practical benefits. In particular, novel thermoelectric materials are materials that exhibit enhanced and attractive thermoelectric behaviors [1] such as higher electrical conductivity, lower thermal conductivity, or generally unique thermoelectric signatures such as the anomalous Nernst effect found in strongly spin-orbit-coupled materials [2–8]. The Nernst effect [9–11] provides evidence of mobile vortices in superconductors [12–15]. Fundamentally, the quasiparticle thermopower (Seebeck effect) provides a different test of the carrier types [16], and the quasiparticle Nernst effects are observed in semimetals with small Fermi surfaces [17]. The thermoelectric effect thus provides unique insight into the underlying physical properties of kagome materials [18,19] and other strongly correlated electron materials [20].

Thermoelectric transport provides a particularly sensitive probe of electronic structure changes associated with symmetry-breaking transitions, because both the Seebeck and Nernst coefficients depend on the energy derivative of the electrical conductivity near the Fermi level. As a result, relatively modest Fermi-surface reconstructions or changes in carrier compensation can generate pronounced thermoelectric signatures even when corresponding changes in longitudinal resistivity are subtle.

The kagome material FeGe (the B35 phase) was reported to host a charge density wave (CDW) transition around 100 K in the antiferromagnetic phase [21–24]. Evidence for this transition has been observed with scanning tunneling microscopy [22], photoemission spectroscopy [23,25,26], magnetic susceptibility, heat capacity, and the electrical transport measurements [21]. There is also a strong spin-lattice-charge coupling across the CDW transition [27]. The amorphous and thin films of the cubic (the B20 phase) FeGe samples have been reported to exhibit the anomalous Hall effect [28,29]. However, the anomalous Hall effect in kagome lattice FeGe was only found at a temperature well below the CDW transition, where spin density wave order was established below T_{cant} ($T_{\mathrm{cant}} < T_{\mathrm{CDW}}$) [30–36]. In addition, the suppressibility of CDW in kagome FeGe has been investigated, specifically with regard to annealing-induced CDW suppression and its effects on magnetic ordering [32–36].

However, despite the evidence for unique thermoelectric behavior in other topological and kagome compounds [37–43], Weyl materials [44–46], and evidence of anomalous Nernst effects and novel thermoelectric behavior in various ferrous materials [47–51], published observations regarding the unique thermoelectric features linked to the charge and

*Contact author: luli@umich.edu

magnetic ordering present in this compound are lacking. In particular, a question remains as to whether there are any sharp features in transport properties associated with the transitions. This paper seeks to fill this gap. Additionally, this work seeks to identify the role of disorder in both thermal behavior and magnetic ordering, as disorder has been shown to influence Nernst effects [52]. We report the finding of a strong Nernst effect in kagome FeGe, providing evidence of its features for the proposed CDW. We demonstrate here that kagome FeGe exhibits evidence of a charge density wave in thermopower measurements and a strong Nernst effect, and that this behavior is strongly suppressed when CDW order is removed through the process of high-temperature annealing [32–35]. We also provide evidence here for magnetic disordering when the CDW feature is suppressed.

In kagome FeGe under appropriate annealing conditions, recent Hall and anomalous Hall transport measurements have already demonstrated a substantial reconstruction of the electronic structure below the CDW transition and the emergence of strongly modified transverse transport in the magnetically ordered state [26,35]. Motivated by these results, we focus here on thermoelectric transport as a complementary and highly sensitive probe of CDW formation and disorder in FeGe.

II. EXPERIMENTAL METHODS

Single crystals were grown using Sn flux, and then annealed in separate batches under different temperature conditions. One batch was annealed at 320 °C for 96 h, and another batch was annealed at 560 °C for 96 h [35]. The orientation of the annealed samples was confirmed using X-ray diffraction. Samples were cut and polished to approximately 1 mm × 0.5 mm × 0.1 mm, perpendicular to the c axis, and each was mounted on a copper block as a heat bath. Thermocouple type-E wires and gold-wire electrical contacts were mounted along the a-b plane. The negative Constantan leads were electrically shorted together. A 1-kΩ resistor was mounted on top of the sample to provide the necessary heat gradient for the measurement, and a layer of thermal epoxy was applied between the sample and the heater to prevent electrical contact. Each lead was mounted to its own nylon pillar using silver epoxy, and the electrical and thermal contacts were made to the physical property measurement system (PPMS) puck using silver paint. Thermal epoxy was applied to each of the thermocouple joints, which were adhered to the sample without making electrical contact. This experimental setup is illustrated in Fig. 1, along with the FeGe crystal structure.

Measurements were taken using a quantum design physical property measurement system (PPMS) Dynacool with a maximum field of 14 T. The magnetic field is oriented normal to the crystal plane surface. In FeGe, a square wave current excitation with an amplitude of 1.6 mA and a frequency of 0.04 Hz was utilized to energize the heater. The Nernst effect is measured perpendicular to the direction of the temperature gradient, and the Seebeck effect is measured along the direction of the temperature gradient. Each thermoelectric voltage signal was obtained by subtracting the bottom, heater-off signal, from the top, heater-on signal. The experiment for each sample consisted of several fixed-temperature field sweeps, varying the temperature in 5 K increments until after the anticipated 100 K charge density wave, and then with a slightly coarser temperature granulation after this feature.

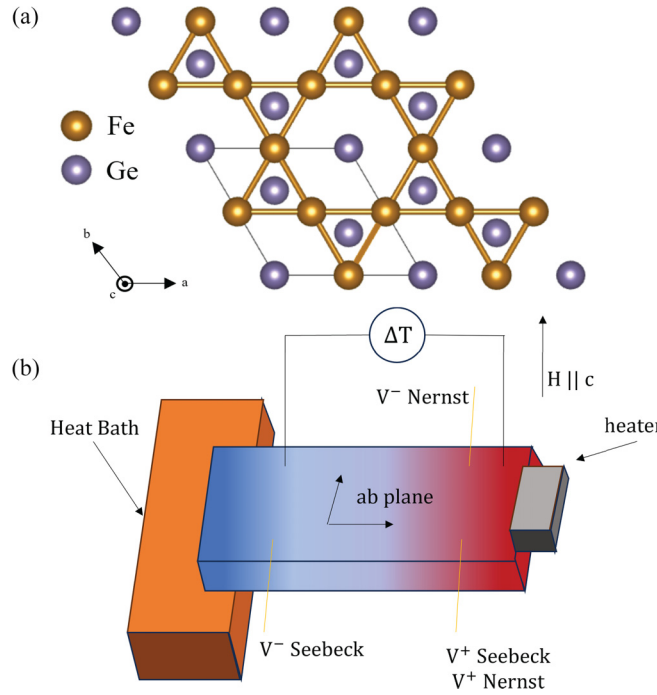

FIG. 1. (a) Crystal structure of Kagome magnet FeGe. (b) Experimental configuration for FeGe thermoelectric measurement. Gold leads indicate electrical contacts, with the sign convention labeled. The sample is oriented with the magnetic field applied along the crystal c axis.

III. RESULTS AND DISCUSSION

The signal evolutions of the Seebeck signal, S_{xx}, for both conditions as a function of temperature and magnetic field are shown in Fig. 2. As can be noted in Fig. 2(a), the thermopower signal shows a distinct curvature change in its magnetic field dependence that evolves with temperature—first appearing at ∼5 T at low temperatures, and shifting gradually to ∼9 T at higher temperatures.

Comparing our data with early reports, we identify this feature with the spin-flop transition [32,35,36]. This feature appears to be present in the 320 °C annealed sample, but does not appear qualitatively similar in the thermopower data for the 560 °C annealed sample, although the field-induced spin-flop transition occurs in both samples [35]. There is some curvature that occurs in the thermopower data for the 560 °C annealed sample, but the field dependence here is not as well defined. The small magnitude of both of these signals and their corresponding noise levels should be taken into consideration as a possible caveat for the exact field dependence of this feature. Also of note regarding the signal strength, the magnitude of the thermopower signal is an order of magnitude larger for the 320 °C sample for $T < T_{\mathrm{CDW}}$, but is of a similar order of magnitude for $T > T_{\mathrm{CDW}}$.

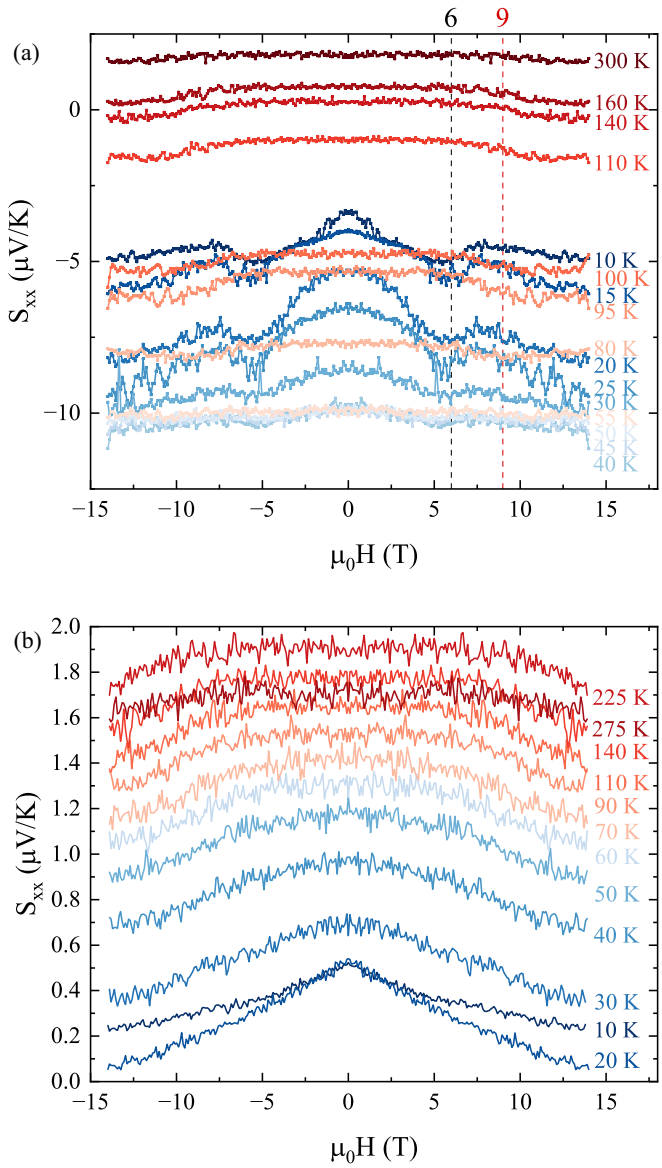

FIG. 2. Thermopower signal S_{xx} of (a) the 320 °C annealed sample as a function of the magnetic field at selected temperatures, and (b) the 560 °C annealed sample as a function of the magnetic field at selected temperatures.

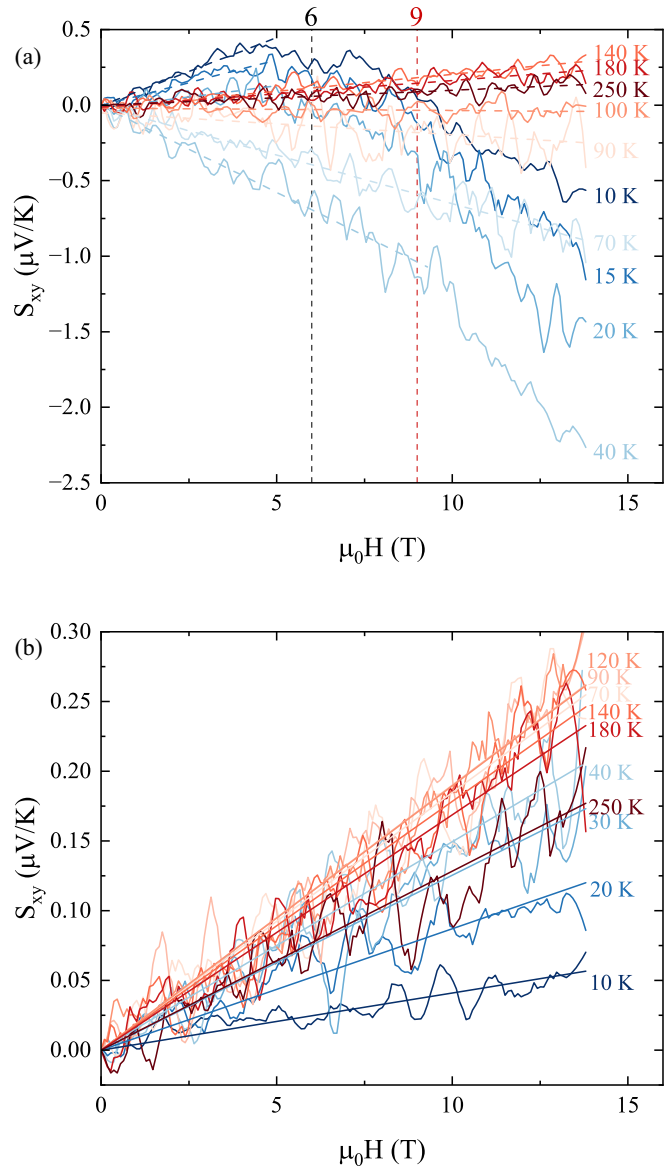

FIG. 3. Nernst signal S_{xy} of (a) the 320 °C annealed sample as a function of the magnetic field at selected temperatures, along with selected linear fits as dotted lines, and (b) 560 °C annealed sample as a function of the magnetic field at selected temperatures, plotted alongside linear fits of the antisymmetrized transverse signal for clarity, as well as defining the Nernst coefficient ν.

To understand the trend of the Nernst effect in this material and its dependence on annealing, fixed-temperature field sweeps were performed for several different temperatures. After deriving the raw Nernst signal $S^0_{xy}(H)$ from the raw signal, the signal was antisymmetrized according to $\frac{S^0_{xy}(H)-S^0_{xy}(-H)}{2}$, with H the applied magnetic field applied along the c axis. This is done to isolate the true Nernst component of the signal and to remove any artifacts or contributions from the longitudinal voltage. The resulting Nernst effect signal S_{xy} for each of the annealing conditions is shown in Figs. 3(a) and 3(b). Furthermore, the zero-field slope of $S_{xy} - \mu_0 H$ is defined as the Nernst coefficient ν, which will be discussed later.

The Nernst effect in both annealed samples has a generally linear trend, with some curvature appearing in the signal from the 320 °C annealed sample for temperatures below the onset of magnetic canting. Again, this curvature appears to correspond to the previously noted spin-flop feature, and the slope has its largest magnitude at ∼50 K before sharply changing inflection. This trend is notably absent in the 560 °C annealed sample signal, which does appear to have a maximum slope around 120 K, but then decreases in magnitude, and does not exhibit any other notable magnetic features. In addition to the general linear trend, the 320 °C signal also exhibits a bump feature around 6 T, which is strongest between 40 and 45 K, and evolves with increasing temperature. This feature is likely a consequence of the 6 T spin-flop phase. However, as this signal is small, the noise is too prominent to see evidence of the 9 T spin-flop transition. The bump feature noted in the

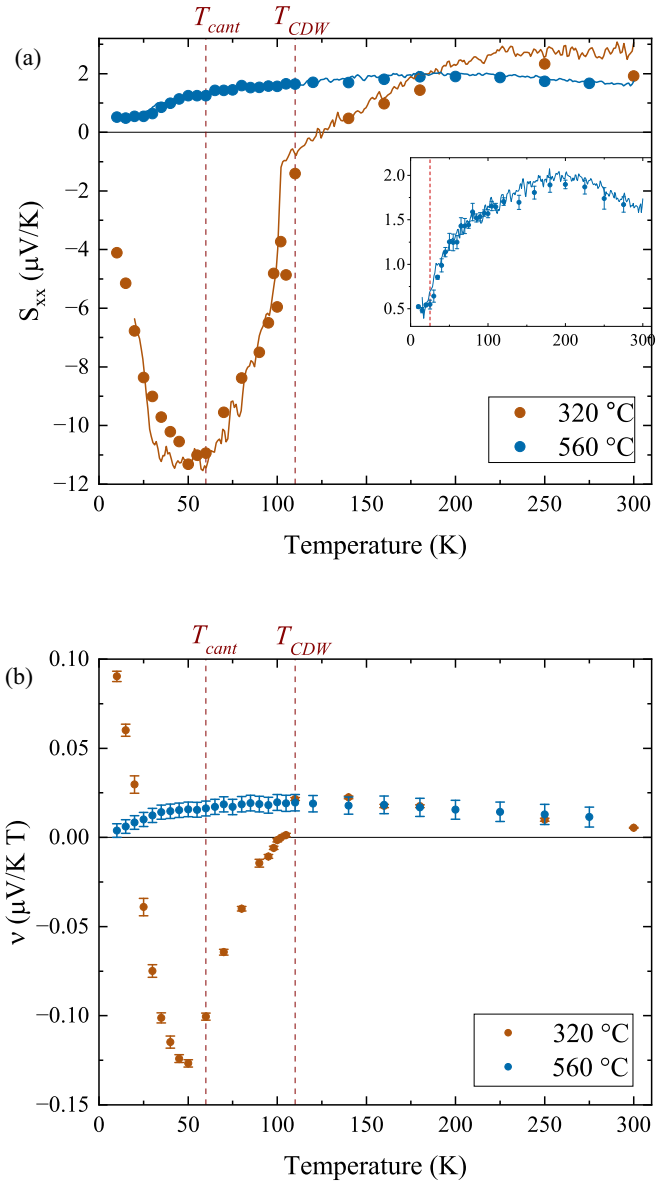

FIG. 4. (a) Seebeck coefficient S_{xx} for both annealing conditions with zero-field temperature sweep curves and (inset) Seebeck coefficient and zero-field temperature sweep for the 560 °C annealed sample, with the literature reported canting temperature marked. (b) Nernst coefficient ν for both conditions in magnetic fields up to 14 T. The heat current is applied along the *ab* plane, and the Seebeck data points were obtained from the zero-field values of the longitudinal voltage extracted from field sweeps at fixed temperatures, normalized by the sample geometry and the temperature gradient across the sample.

320 °C sample does not appear to be present under the 560 °C annealing condition.

Further analysis of these trends can be observed in Fig. 4(a), which displays the zero-field thermopower S_{xx} as a function of temperature for each annealing condition, and Fig. 4(b), which shows ν for each annealing condition as a function of temperature. The field-dependent Seebeck coefficient $S_{xx}(H)$ was extracted from the zero-field intercepts of the symmetrized field sweeps at fixed temperature. For the Nernst coefficient, linear fits were applied to $S_{xy}(H)$ over a restricted low-field window below the onset of the spin-flop feature in the 320 °C annealed sample, while the full field range was used for the 560 °C annealed sample. Statistical uncertainties of these linear fits are shown as error bars in $\nu(T)$. Both figures show remarkably similar features in both S_{xx} and ν, with the 560 °C annealed sample remaining exclusively positive, and the 320 °C annealed sample changing sign close to $T = T_{\mathrm{CDW}}$ at ∼120 K. Both of these samples share holelike charge carriers at room temperature, which we define here as a positive Seebeck signal.

Furthermore, a rapid slope change appears to occur in S_{xy} for the 320 °C annealed sample in the vicinity of the charge density wave transition, and S_{xx} exhibits a kink feature near T_{CDW}, which we observe close to 110 K. This sign change is clearly absent in the sample annealed at 560 °C. In the CDW-containing sample, this trend continues for the temperature range $T_{\mathrm{CDW}} < T < 300$ K. For $T < T_{\mathrm{CDW}}$, the sample exhibits a sizable negative (electronlike) thermopower signal, indicating that electronlike contributions dominate the thermoelectric response in the CDW state. Holes become the dominant quasiparticle charge carriers at ∼120 K, when S_{xx} is positive in Fig. 4(a). The temperature of the sign change in S_{xx} follows T_{CDW} by about 10 K, a picture that is consistent with a gradual evolution of the chemical potential, scattering rates, or more general Fermi-surface reconstruction associated with CDW formation. Thus, the sign change in S_{xx} is not a sharp first-order transition at a single temperature. However, the magnitude of S_{xx} experiences its largest change for $T < T_{\mathrm{CDW}}$. By contrast, the absence of any comparable anomaly in the 560 °C annealed sample indicates that disorder suppresses both long-range CDW coherence and the associated energy-dependent transport asymmetry.

Recent neutron scattering and susceptibility measurements on annealed FeGe demonstrate that while long-range CDW order is strongly suppressed by high-temperature annealing (such as 560 °C), the incommensurate antiferromagnetic phase persists to a lower characteristic temperature in the absence of CDW order [36]. Annealing-induced Ge vacancies reduce the onset temperature of this incommensurate magnetic order but do not eliminate it, indicating that the incommensurate spin configuration is an intrinsic magnetic instability that survives even without static CDW order [35]. T_{cant} is pushed to ∼25 K, which is where we also note the greatest inflection in ν [see Fig. 4(a) inset].

Figure 4(a) shows that only the 320 °C annealed sample, which hosts long-range CDW order, exhibits a large enhancement and sign reversal of the Seebeck coefficient. In contrast, the 560 °C annealed sample, in which CDW coherence is suppressed by disorder, displays a smooth, weakly temperature-dependent, and strictly positive thermopower. This strongly implicates CDW-induced Fermi-surface reconstruction as the primary origin of the thermopower reversal and large low-temperature magnitude. Although a subtle change in slope of $S_{xx}(T)$ is visible near the canting temperature, no additional sign change or abrupt enhancement is observed at this magnetic transition. This indicates that the onset of noncollinear magnetism provides only a secondary renormalization of the thermoelectric response, likely through modest band reshaping and scattering changes, while

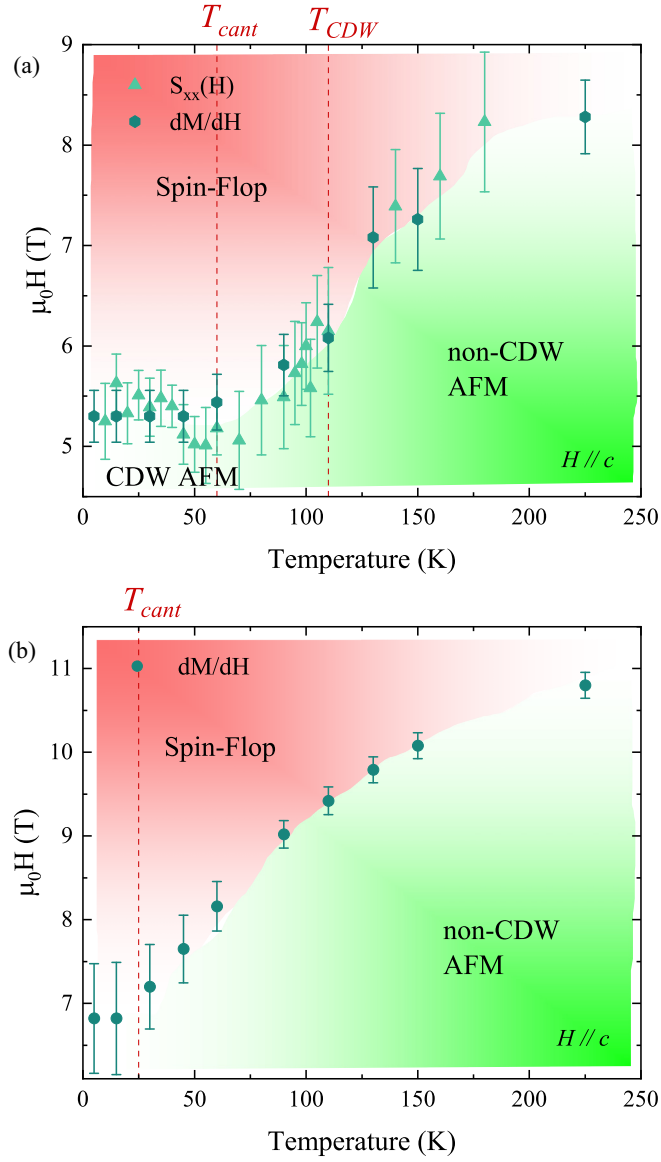

FIG. 5. The phase diagram of $\mu_0 H$ vs T for (a) the 320 °C annealed sample and (b) the 560 °C annealed sample, using the locations of various magnetic features to define the phase transitions. The boundaries of the canted antiferromagnetic (AFM) phase and CDW-ordered phase are delineated here as T_{cant} and T_{CDW}, respectively.

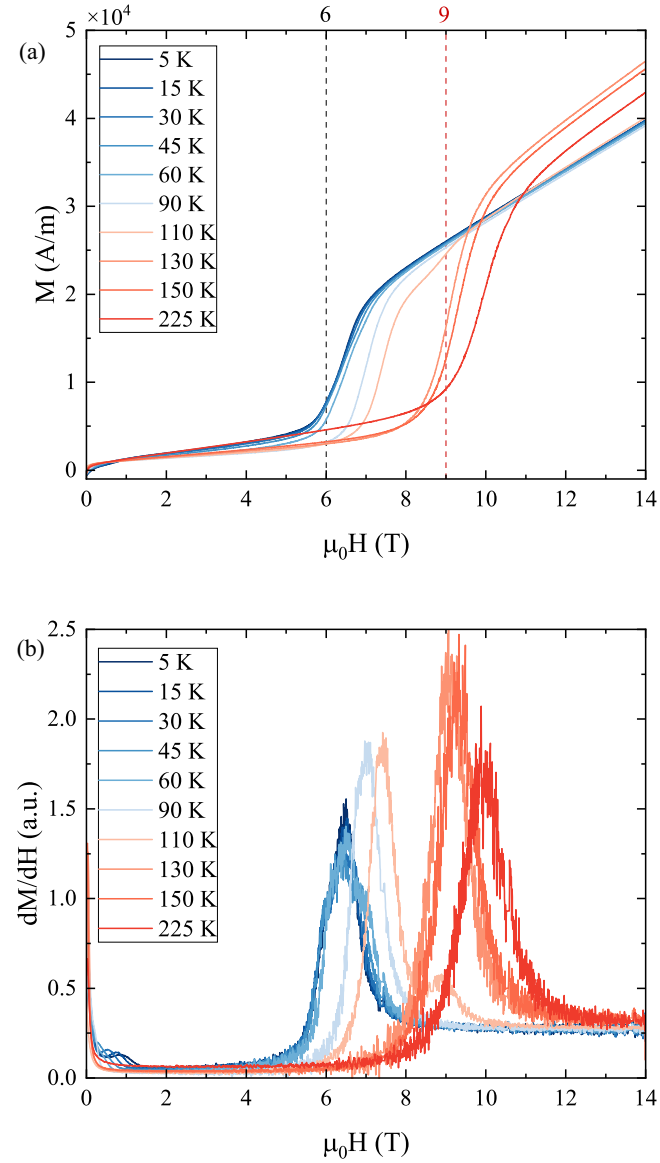

FIG. 6. Magnetization as a function of magnetic field for the 320 °C annealed sample (a) plotted alongside dM/dH (b).

the dominant thermoelectric reconstruction is driven by CDW formation. Within this coupled-order framework, incommensurate magnetic order renormalizes the low-temperature electronic state but does not by itself generate the enhanced thermopower. Thus, we conclude that incommensurate magnetic order leaves a thermoelectric fingerprint, but does not control the sign or main enhancement of S_{xx}. The CDW is the primary driver of both the sign change and the large low-temperature thermopower, while incommensurate magnetic order provides only a secondary renormalization of the thermoelectric response.

Similarly, the Nernst coefficient ν exhibits a similar trend in T. For $T < T_{\text{CDW}}$, the sample exhibiting the CDW shows a much more sizable Nernst coefficient in the opposite sign than that after the CDW transition. The Nernst coefficient ν-T is plotted in Fig. 4(b). Notably, ν for the 320 °C annealed sample is significantly larger than that of the 560 °C annealed sample. This signal has a peak at ∼50 K, and changes sign around 105 K. The absolute magnitude of the Nernst coefficient in the 320 °C annealed sample is almost 22× larger than the 560 °C sample at its largest magnitude as well. We also note that the 320 °C annealed sample has much stronger incommensurate magnetic peaks associated with spin density wave order below 60 K which are considerably suppressed for the 560 °C annealed sample [35]. These findings are further examined in the phase diagrams shown in Figs. 5(a) and 5(b).

We construct H-T diagrams using a combination of the spin-flop affiliated inflections in $S_{xx}(H)$ and $M(H)$ data. We note that the phase diagrams shown for each sample are both numerically and characteristically different. In Fig. 5(a), we notice the spin-flop feature remains roughly localized for $T < T_{\text{cant}}$, and then increases smoothly and monotonically for

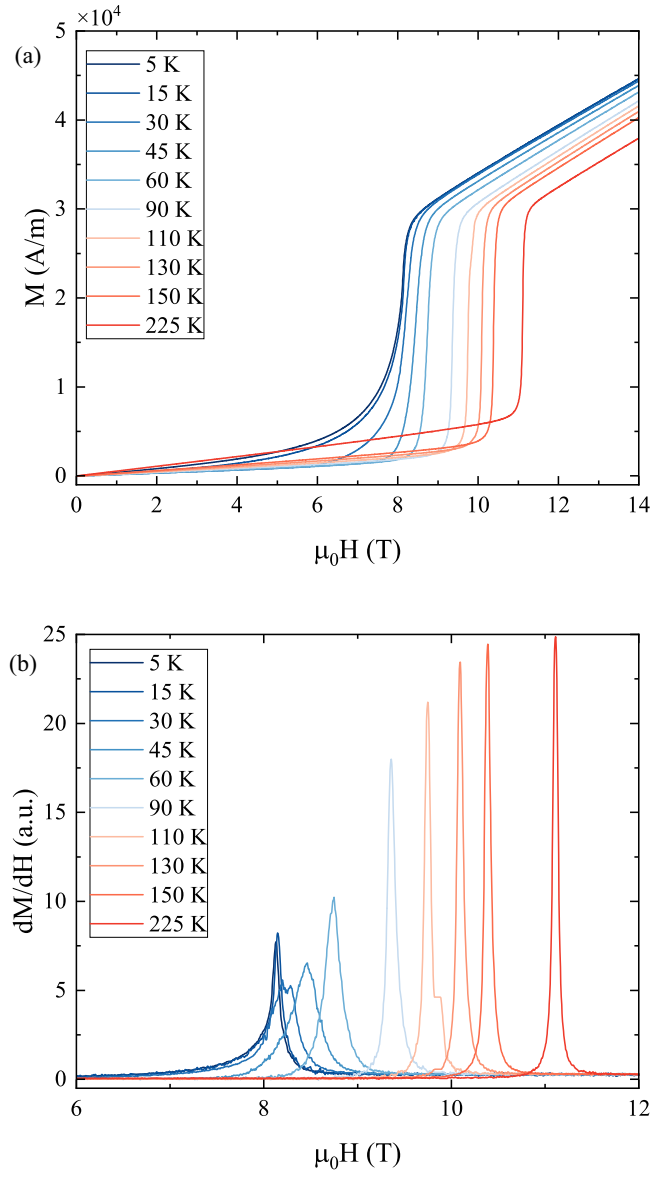

FIG. 7. Magnetization as a function of magnetic field for the 560 °C annealed sample (a) plotted alongside dM/dH (b).

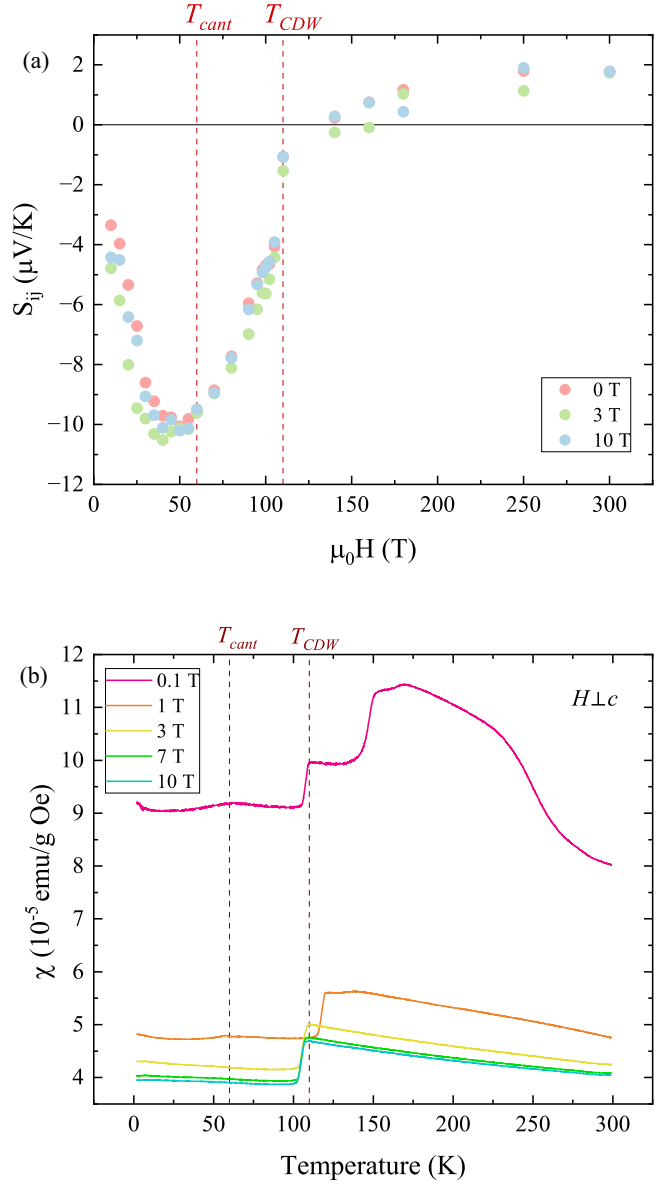

FIG. 8. (a) Seebeck coefficient $S_{xx}(T)$ of the 320 °C annealed sample extracted from the set-field values of fixed-temperature field sweeps at 0, 3, and 10 T fields. The sign change of $S_{xx}(T)$ remains sharp and essentially field independent, demonstrating that the thermopower reversal is not associated with the field-fragile magnetic anomaly near 140 K. (b) Magnetic susceptibility $\chi(T)$ under the same annealing condition measured at fixed magnetic fields, showing a weak anomaly near $T \approx 140$ K that rapidly smears out with increasing field.

$T > T_{\text{cant}}$. Unlike the sign change we see in both the Seebeck and Nernst effects, there are no sharp features that occur in H-T at $T = T_{\text{CDW}}$. Likewise, the 560 °C annealed sample reveals the same qualitative phase topology—a low-temperature incommensurate phase, and a field-induced spin-flop transition for $H \parallel c$. Quantitatively, Fig. 5(b) demonstrates a slight shift of the spin flop to higher fields while T_{cant} is pushed to a lower temperature. However, all characteristic scales are systematically enhanced in the CDW-hosting sample: the canting temperature is higher, the spin-flop field is larger at all temperatures, and the magnetic anomalies are sharper.

The H-T phase diagram of annealed FeGe is organized by the emergence of a low-temperature canted or incommensurate antiferromagnetic phase, which persists even when long-range CDW order is suppressed by annealing. This indicates that incommensurate order is an intrinsic magnetic instability rather than a direct consequence of CDW formation. However, CDW coherence systematically renormalizes the temperature and field scales associated with this instability: samples hosting long-range CDW order exhibit a higher canting temperature, an enhanced spin-flop field, and sharper magnetic transitions. This behavior is naturally understood in terms of CDW-induced Fermi-surface reconstruction, which modifies the electronic contribution to the magnetic free energy and thereby renormalizes the stability of the noncollinear magnetic state without generating new magnetic phases.

Previous works have also asserted the presence of incommensurate magnetic Bragg peaks around 60 K [21,23,32], which is also supported by our measurements and labeled here as T_{cant}. It is interesting to point out that recent photoemission work has also identified changes in the electronic structure at this characteristic temperature scale in the 320 °C annealed sample, while absent in the 560 °C annealed sample [25], consistent with the trends of S_{xx} and ν.

IV. CONCLUSIONS

In conclusion, in the Kagome metal FeGe, this thermoelectric effect study demonstrates a dramatic change in electronic structure accompanying the CDW transition. Compared to the crystal without the CDW transition, the crystal with the CDW is revealed to have a significantly enhanced Nernst effect and a dramatic sign change of the dominant carrier in the thermopower effect. This result suggests that the disorder created by the annealing conditions in Ge-1 site may prevent the CDW formation [35]. Thermoelectric effects are also shown to detect the spin-flop transition and the onset of spin canting. While T_{cant} leaves a measurable thermoelectric fingerprint in both samples, the dominant reconstruction of the thermoelectric response is driven by CDW formation, while canting provides only a secondary renormalization.

ACKNOWLEDGMENTS

The work at the University of Michigan is supported by the National Science Foundation under Awards No. DMR-2004288 and No. DMR-2317618 (transport measurements), by the Department of Energy under Award No. DE-SC0020184 (magnetization measurements) to K.-W.C., D.Z., G.Z., A.C., Y.Z., K.J., and L.L. The single-crystal synthesis and characterization at Rice are supported by U.S. NSF Grant No. DMR-2401084 and the Robert A. Welch Foundation under Grant No. C-1839 (P.D.).

DATA AVAILABILITY

The data that support the findings of this article are openly available [53].

APPENDIX

To further investigate and contrast the magnetic transitions in FeGe under varying amounts of disorder, the magnetization for each annealing condition was contrasted. A portion of the information shown in these figures is reflected in the phase diagrams shown in Fig. 5. Specifically, the points of inflection in dM/dH before the peaks are used in part to formulate the phase information for both annealing conditions. The magnetization trends for both samples are displayed in Figs. 6 and 7, alongside the corresponding dM/dH for each condition. There is a distinct shift in the magnetization of the 320 °C annealed sample in the temperature range $90 < T < 130$ K, specifically observable in the 110 K curve. This observation is not present in the 560 °C annealed sample, where dM/dH shifts monotonically and increases in sharpness with increasing temperature. The spin-flop phase seen in Fig. 5 reflects the ordered state after the spin flop has taken place, and the AFM phase describes the region in the magnetization at lower fields, prior to the rapid change in magnetization.

A weak magnetic anomaly is also observed near $T \approx 140$ K in the 320 °C annealed sample, raising the question of whether this feature could influence the observed thermopower reversal. To address this possibility directly, Fig. 8 compares the temperature dependence of the magnetic susceptibility and the Seebeck coefficient for this sample under applied magnetic fields. The susceptibility anomaly near 140 K is rapidly suppressed with increasing field, whereas the Seebeck coefficient retains a sharp and well-defined sign change that is essentially field independent. This contrasting field response demonstrates that the thermopower reversal cannot originate from the 140 K magnetic feature. Instead, the robustness of the Seebeck sign change against the magnetic field is consistent with an electronic reconstruction driven by CDW formation, rather than by a field-fragile magnetic instability.

[1] *Thermal Conductivity: Theory, Properties, and Applications*, edited by T. M. Tritt (Springer Science & Business Media, New York, 2004).

[2] N. Nagaosa, J. Sinova, S. Onoda, A. H. MacDonald, and N. P. Ong, Anomalous Hall effect, Rev. Mod. Phys. **82**, 1539 (2010).

[3] S. Onoda, N. Sugimoto, and N. Nagaosa, Quantum transport theory of anomalous electric, thermoelectric, and thermal Hall effects in ferromagnets, Phys. Rev. B **77**, 165103 (2008).

[4] M. Ikhlas, T. Tomita, T. Koretsune, M.-T. Suzuki, D. Nishio-Hamane, R. Arita, Y. Otani, and S. Nakatsuji, Large anomalous Nernst effect at room temperature in a chiral antiferromagnet, Nat. Phys. **13**, 1085 (2017).

[5] H. Yang, W. You, J. Wang, J. Huang, C. Xi, X. Xu, C. Cao, M. Tian, Z.-A. Xu, J. Dai, *et al.*, Giant anomalous Nernst effect in the magnetic Weyl semimetal $Co_3Sn_2S_2$, Phys. Rev. Mater. **4**, 024202 (2020).

[6] S. N. Guin, P. Vir, Y. Zhang, N. Kumar, S. J. Watzman, C. Fu, E. Liu, K. Manna, W. Schnelle, J. Gooth, *et al.*, Zero-field Nernst effect in a ferromagnetic kagome-lattice Weyl-semimetal $Co_3Sn_2S_2$, Adv. Mater. **31**, 1806622 (2019).

[7] R. P. Madhogaria, S. Mozaffari, H. Zhang, W. R. Meier, S.-H. Do, R. Xue, T. Matsuoka, and D. G. Mandrus, Topological Nernst and topological thermal Hall effect in rare-earth kagome $ScMn_6Sn_6$, Phys. Rev. B **108**, 125114 (2023).

[8] H. Zhang, C. Q. Xu, and X. Ke, Topological Nernst effect, anomalous Nernst effect, and anomalous thermal Hall effect in the Dirac semimetal Fe_3Sn_2, Phys. Rev. B **103**, L201101 (2021).

[9] K. Behnia, The Nernst effect and the boundaries of the Fermi liquid picture, J. Phys.: Condens. Matter **21**, 113101 (2009).

[10] K. Behnia and H. Aubin, Nernst effect in metals and superconductors: A review of concepts and experiments, Rep. Prog. Phys. **79**, 046502 (2016).

[11] E. H. Sondheimer, The theory of the galvanomagnetic and thermomagnetic effects in metals, Proc. R. Soc. London, Ser. A **193**, 484 (1948).

[12] Z. Zhu, H. Yang, B. Fauque, Y. Kopelevich, and K. Behnia, Nernst effect and dimensionality in the quantum limit, Nat. Phys. **6**, 26 (2010).

[13] Y. Wang, L. Li, and N. P. Ong, Nernst effect in high-T_c superconductors, Phys. Rev. B **73**, 024510 (2006).

[14] Y. Onose, L. Li, C. Petrovic, and N. P. Ong, Anomalous thermopower and Nernst effect in $CeCoIn_5$: Loss of entropy current in precursor state, Europhys. Lett. **79**, 17006 (2007).

[15] L. Chen, Z. Xiang, C. Tinsman, B. Lei, X. Chen, G. D. Gu, and L. Li, Spontaneous Nernst effect in the iron-based superconductor $Fe_{1+y}Te_{1-x}Se_x$, Phys. Rev. B **102**, 054503 (2020).

[16] J. M. Ziman, *Electrons and Phonons: The Theory of Transport Phenomena in Solids* (Oxford University Press, Oxford, UK, 2001).

[17] K. Behnia, *Fundamentals of Thermoelectricity* (Oxford University Press, Oxford, UK, 2015).

[18] Y.-X. Jiang, J.-X. Yin, M. M. Denner, N. Shumiya, B. R. Ortiz, G. Xu, Z. Guguchia, J. He, M. S. Hossain, X. Liu, J. Ruff, L. Kautzsch, S. S. Zhang, G. Chang, I. Belopolski, Q. Zhang, T. A. Cochran, D. Multer, M. Litskevich, Z.-J. Chang, *et al.*, Unconventional chiral charge order in kagome superconductor KV_3Sb_5, Nat. Mater. **20**, 1353 (2021).

[19] X. Xu, J. Yin, Z. Qu, and S. Jia, Quantum interactions in topological R166 kagome magnet, Rep. Prog. Phys. **86**, 114502 (2023).

[20] P. Sun and F. Steglich, Nernst effect: Evidence of local Kondo scattering in heavy fermions, Phys. Rev. Lett. **110**, 216408 (2013).

[21] X. Teng, L. Chen, F. Ye, E. Rosenberg, Z. Liu, J. X. Yin, Y.-X. Jiang, J. S. Oh, M. Z. Hasan, K. Neubauer, B. Gao, Y. Xie, M. Hashimoto, D. Lu, C. Jozwiak, A. Bostwick, E. Rotenberg, R. J. Burgeneau, J.-H. Chu, M. Yi, *et al.*, Discovery of charge density wave in a kagome lattice antiferromagnet, Nature (London) **609**, 490 (2022).

[22] J.-X. Yin, Y.-X. Jiang, X. Teng, M. S. Hossain, S. Mardanya, T.-R. Chang, Z. Ye, G. Xu, M. M. Denner, T. Neupert, B. Lienhard, H.-B. Deng, C. Setty, Q. Si, G. Chang, Z. Guguchia, B. Gao, N. Shumiya, Q. Zhang, T. A. Cochran, *et al.*, Discovery of charge order and corresponding edge state in kagome magnet FeGe, Phys. Rev. Lett. **129**, 166401 (2022).

[23] X. Teng, J. S. Oh, H. Tan, L. Chen, J. Huang, B. Gao, J. X. Yin, J.-H. Chu, M. Hashimoto, D. Lu, C. Jozwiak, A. Bostwick, E. Rotenberg, G. Granroth, B. Yan, R. J. Burgeneau, P. Dai, and M. Yi, Magnetism and charge density wave order in kagome FeGe, Nat. Phys. **19**, 814 (2023).

[24] S. Shao, J.-X. Yin, I. Belopolski, J.-Y. You, T. Hou, H. Chen, Y. Juang, M. S. Hossain, M. Yahyavi, C.-H. Hsu, Y. P. Feng, A. Bansil, M. Z. Hasan, and G. Chang, Intertwining of magnetism and charge ordering in kagome FeGe, ACS Nano **17**, 10164 (2023).

[25] J. Oh, A. Biswas, M. Klemm, H. Tan, Y. Xie, B. Gao, M. Hashimoto, D. Lu, B. Yan, P. Dai, R. J. Birgeneau, and M. Yi, Disentangling the intertwined orders in a magnetic kagome metal, Sci. Adv. **11**, eadt2195 (2025).

[26] Z. Zhao, T. Li, P. Li, X. Wu, J. Yao, Z. Chen, S. Cui, Z. Sun, Y. Yang, Z. Jiang, Z. Liu, A. Louat, T. Kim, C. Cacho, A. Wang, Y. Wang, D. Shen, J. Jiang, and D. L. Feng, Photoemission evidence of a novel charge order in kagome metal FeGe, Sci. China Phys. Mech. Astron. **68**, 267012 (2025).

[27] X. Teng, D. W. Tam, L. Chen, H. Tan, Y. Xie, B. Gao, G. E. Granroth, A. Ivanov, P. Bourges, B. Yan, M. Yi, and P. Dai, Spin-charge-lattice coupling across the charge density wave transition in a kagome lattice antiferromagnet, Phys. Rev. Lett. **133**, 046502 (2024).

[28] D. S. Bouma, Z. Chen, B. Zhang, F. Bruni, M. E. Flatté, A. Ceballos, R. Streubel, L.-W. Wang, R. Q. Wu, and F. Hellman, Itinerant ferromagnetism and intrinsic anomalous Hall effect in amorphous iron-germanium, Phys. Rev. B **101**, 014402 (2020).

[29] N. A. Porter, J. C. Gartside, and C. H. Marrows, Scattering mechanisms in textured FeGe thin films: Magnetoresistance and the anomalous Hall effect, Phys. Rev. B **90**, 024403 (2014).

[30] J. Bernhard, B. Lebech, and O. Beckman, Neutron diffraction studies of the low-temperature magnetic structure of hexagonal FeGe, J. Phys. F: Met. Phys. **14**, 2379 (1984).

[31] L. Chen, X. Teng, H. Tan, B. L. Winn, G. E. Granroth, F. Ye, D. H. Yu, R. A. Mole, B. Gao, B. Yan, M. Yi, and P. Dai, Competing itinerant and local spin interactions in kagome metal FeGe, Nat. Commun. **15**, 1918 (2024).

[32] X. Wu, X. Mi, L. Zhang, C.-W. Wang, N. Maraytta, X. Zhou, M. He, M. Merz, Y. Chai, and A. Wang, Annealing-tunable charge density wave in the kagome antiferromagnet FeGe, Phys. Rev. Lett. **132**, 256501 (2024).

[33] Z. Chen, X. Wu, S. Zhou, J. Zhang, R. Yin, Y. Li, M. Li, J. Gong, M. He, Y. Chai, X. Zhou, Y. Wang, A. Wang, Y.-J. Yan, and D.-L. Feng, Discovery of a long-ranged charge order with 1/4 Ge1-dimerization in an antiferromagnetic Kagome metal, Nat. Commun. **15**, 6262 (2024).

[34] C. Shi, Y. Liu, B. B. Maity, Q. Wang, S. R. Kotla, S. Ramakrishnan, C. Eisele, H. Agarwal, L. Noohinejad, Q. Tao, B. Kang, Z. Lou, X. Yang, Y. Qi, X. Lin, Z.-A. Xu, A. Thamizhavel, G.-H. Cao, S. van Smaalen, S. Cao, and J.-K. Bao, Annealing-induced long-range charge density wave order in magnetic kagome FeGe: Fluctuations and disordered structure, Sci. China Phys. Mech. Astron. **67**, 117012 (2024).

[35] M. Klemm, S. Siddique, Y.-C. Chang, S. Xu, Y. Xie, T. Legvold, M. T. Kiani, F. Ye, H. Cao, Y. Hao, W. Tian, H. Luetkens, M. Matsuda, D. Natelson, Z. Guguchia, C.-L. Huang, M. Yi, J. J. Cha, and P. Dai, Vacancy-induced suppression of CDW order and its impact on magnetic order in kagome antiferromagnet FeGe, Nat. Commun. **16**, 3313 (2025).

[36] M. L. Klemm, T. Zhang, B. L. Winn, F. Li, F. Ye, M. Matsuda, A. Maity, S. Xu, X. Teng, Y. Umemoto, B. Gao, M. Yi, and P. Dai, Interacting spin and charge density waves in the kagome metal FeGe, Phys. Rev. B **112**, 174422 (2025).

[37] Y. Zhu, D. Zhang, G. Zheng, K.-W. Chen, H. Bhandari, K. Jenkins, A. Chan, N. J. Ghimire, and L. Li, Geometrical Nernst effect in the kagome magnet $YMn_6Sn_4Ge_2$, Phys. Rev. B **110**, 195125 (2024).

[38] T. Asaba, V. Ivanov, S. M. Thomas, S. Y. Savrasov, J. D. Thompson, E. D. Bauer, and F. Ronning, Colossal anomalous Nernst effect in a correlated noncentrosymmetric kagome ferromagnet, Sci. Adv. **7**, eabf1467 (2021).

[39] S. Roychowdhury, A. M. Ochs, S. N. Guin, K. Samanta, J. Noky, C. Shekhar, M. G. Vergniory, J. E. Goldberger, and

C. Felser, Large room temperature anomalous transverse thermoelectric effect in kagome antiferromagnet YMn_6Sn_6, Adv. Mater. **34**, 2201350 (2022).

[40] H. Bhandari, R. L. Dally, P. E. Siegfried, R. B. Regmi, K. C. Rule, S. Chi, J. W. Lynn, I. Mazin, and N. J. Ghimire, Magnetism and fermiology of kagome magnet $YMn_6Sn_4Ge_2$, npj Quantum Mater. **9**, 6 (2024).

[41] C. Zeng, X.-Q. Yu, Z.-M. Yu, and Y. Yao, Band tilt induced nonlinear Nernst effect in topological insulators: An efficient generation of high-performance spin polarization, Phys. Rev. B **106**, L081121 (2022).

[42] M. Ceccardi, A. Zeugner, C. Hess, B. Büchner, D. Marré, A. Isaeva, and F. Caglieris, Anomalous Nernst effect in the topological and magnetic material $MnBi_4Te_7$, npj Quantum Mater. **8**, 76 (2023).

[43] G. Sharma, Tunable topological Nernst effect in two-dimensional transition-metal dichalcogenides, Phys. Rev. B **98**, 075416 (2018).

[44] G. Sharma, C. Moore, S. Saha, and S. Tewari, Nernst effect in Dirac and inversion-asymmetric Weyl semimetals, Phys. Rev. B **96**, 195119 (2017).

[45] S. J. Watzman, T. M. McCormick, C. Shekhar, S.-C. Wu, Y. Sun, A. Prakash, C. Felser, N. Trivedi, and J. P. Heremans, Dirac dispersion generates unusually large Nernst effect in Weyl semimetals, Phys. Rev. B **97**, 161404(R) (2018).

[46] L. Xu, X. Li, L. Ding, T. Chen, A. Sakai, B. Fauqué, S. Nakatsuji, Z. Zhu, and K. Behnia, Anomalous transverse response of Co_2MnGa and universality of the room-temperature $\alpha_{ij}^A/\sigma_{ij}^A$ ratio across topological magnets, Phys. Rev. B **101**, 180404(R) (2020).

[47] W.-L. Lee, S. Watauchi, V. L. Miller, R. J. Cava, and N. P. Ong, Anomalous Hall heat current and Nernst effect in the $CuCr_2Se_{4-x}Br_x$ ferromagnet, Phys. Rev. Lett. **93**, 226601 (2004).

[48] T. Miyasato, N. Abe, T. Fujii, A. Asamitsu, S. Onoda, Y. Onose, N. Nagaosa, and Y. Tokura, Crossover behavior of the anomalous Hall effect and anomalous Nernst effect in itinerant ferromagnets, Phys. Rev. Lett. **99**, 086602 (2007).

[49] Y. Pu, D. Chiba, F. Matsukura, H. Ohno, and J. Shi, Mott relation for anomalous Hall and Nernst effects in $Ga_{1-x}Mn_xAs$ ferromagnetic semiconductors, Phys. Rev. Lett. **101**, 117208 (2008).

[50] T. C. Chuang, P. L. Su, P. H. Wu, and S. Y. Huang, Enhancement of the anomalous Nernst effect in ferromagnetic thin films, Phys. Rev. B **96**, 174406 (2017).

[51] R. Ramos, M. H. Aguirre, A. Anadón, J. Blasco, I. Lucas, K. Uchida, P. A. Algarabel, L. Morellón, E. Saitoh, and M. R. Ibarra, Anomalous Nernst effect of Fe_3O_4 single crystal, Phys. Rev. B **90**, 054422 (2014).

[52] L. Ding, J. Koo, L. Xu, X. Li, X. Lu, L. Zhao, Q. Wang, Q. Yin, H. Lei, B. Yan, Z. Zhu, and K. Behnia, Intrinsic anomalous Nernst effect amplified by disorder in a half-metallic semimetal, Phys. Rev. X **9**, 041061 (2019).

[53] K. Jenkins *et al.*, Thermoelectric evidence of the electronic structure changes from the charge-density-wave transition in FeGe, OSF (2026), https://osf.io/rm824/.